

# High Energy Nucleon Incident Optical Potential by Relativistic Impulse Approximation

Nobuhiro SHIGYO, Kazuo NAKAMURA, Hirohiko KITSUKI and Kenji ISHIBASHI  
*Department of Applied Quantum Physics and Nuclear Engineering, Kyushu University*  
*Hakozaki, Higashi-ku, Fukuoka-shi 812-8581.*  
*e-mail:shigyo@kune2a.nucl.kyushu-u.ac.jp*

The optical potentials by relativistic impulse approximation (RIA) are utilized for the high energy nucleon incidence. The nucleon-nucleon scattering amplitudes are derived from the phase shift and parametrized as a function of the incident nucleon energy. The optical potential by RIA reproduces the experimental data.

## 1. Introduction

It is expected that a number of neutrons generated by the high energy spallation reaction are utilized to engineering purposes such as high intensity neutron source, accelerator-driven transmutation system, accelerator-driven subcritical nuclear reactor and so on. Because of lack of the experimental data of neutron production cross section in the spallation reaction, simulation codes such as Nucleon Meson Transport Code (NMTC) [1] and High Energy Transport Code (HETC) [2] and based on the intranuclear-cascade-evaporation model [3] are often used to the engineering design. Calculation results of the codes, however, is poor agreement with experimental data in the forward direction as near 0 degree. The neutron production cross section in the forward direction is much larger than the backward direction and important in the case such as the shielding calculation of the facility. One of the reason of the disagreement is that HETC is no consideration of the elastic scattering in the forward direction. Improvement of the neutron production cross section in the forward direction, the nucleon-nucleus Dirac optical potential is used. The potential is obtained by the relativistic impulse approximation (RIA) [4]. In RIA the nucleon-nucleus Dirac optical potential is derived from the summation of the nucleon-nucleon scattering amplitude for each nucleon in the target nucleus. The nucleon-nucleon scattering amplitude mainly has five components (scalar, vector, tensor, pseudoscalar and axial vector) [5]. The components except for the scalar and the vector ones are neglected because of small contribution in the energy around 1 GeV. The nucleon-nucleon scattering amplitudes for each orbit are given by fitting empirical phase shift data [6]. To simplify calculation of the potential, the neutron-proton and proton-proton scattering amplitudes are parameterized in a Gaussian shape as a function of the momentum transfer for each incident energy. The Dirac equation is also changed to the Dirac-Schrödinger equation. The neutron production cross section is obtained by solving the equation. The cross sections by this method are good agreement with the experimental data in high incident energy region.

## 2. Relativistic Impulse Approximation

The optical potential is represented by [7]

$$U_{opt}(r) = -\frac{4\pi p_{lab}}{M} \langle \Psi | \hat{F} | \Psi \rangle \quad (1)$$

where,  $p_{lab}$  and  $M$  are the momentum of incident particle in the laboratory frame, and the rest mass, respectively.  $|\Psi\rangle$  is the wave function in the ground state.  $\hat{F}$  is the Dirac scattering amplitude for the relativistic nucleon-nucleus scattering and is represented by

$$\hat{F} = F^S + F^V \gamma_{(0)}^\mu \gamma_{(i)\mu} + F^{PS} \gamma_0^5 \gamma_i^5 + F^T \sigma_{(0)}^{\mu\nu} \sigma_{(i)\mu\nu} + F^A \gamma_{(0)}^5 \gamma_{(0)}^\mu \gamma_{(i)}^5 \gamma_{(i)\mu} \quad (2)$$

where, suffix (0), (i) stand for the incident particle and a particle of the target nucleus, respectively. Suffix  $S$ ,  $V$ ,  $PS$ ,  $T$  and  $A$  are scalar, vector, pseudoscalar, tensor and axial vector, respectively.  $\sigma$  and  $\gamma$  are the Pauli  $\sigma$  matrix and the Dirac  $\gamma$  one, respectively. The pseudoscalar and the axial vector elements

are neglected for the sphere nucleus. The tensor term is smaller than the scalar or the vector terms. Then, the optical potential is represented by

$$\hat{U}_{opt}(q) = -\frac{4\pi i p_{lab}}{M} \left[ \langle \Psi | F^S(q) | \Psi \rangle \rho^S(q) + \gamma_{(0)}^0 \langle \Psi | F^V(q) | \Psi \rangle \rho^V(q) \right] \quad (3)$$

where,  $q$  is the momentum transfer and  $\rho^S(q)$  and  $\rho^V(q)$  are shown as

$$\rho^S(q) = \left\langle \Psi \left| \sum_i^A e^{i\vec{q}\cdot\vec{r}_i} \right| \Psi \right\rangle \quad (4)$$

$$\rho^V(q) = \left\langle \Psi \left| \sum_i^A \gamma_i^0 e^{i\vec{q}\cdot\vec{r}_i} \right| \Psi \right\rangle \quad (5)$$

The scattering amplitude  $F^S$  and  $F^V$  are parametrized as

$$F^S(q) = F_{S0} e^{-q^2 \beta_S} \quad (6)$$

$$F^V(q) = F_{V0} e^{-q^2 \beta_V} \quad (7)$$

where,  $F_{S0}$ ,  $F_{V0}$ ,  $\beta_S$  and  $\beta_V$  are parameters obtained from fitting the nucleon-nucleon scattering cross sections. These parameters are derived from the phase shifts. In this work, the phase shift is obtained by fitting the empirical data [6]. The phase shift of  $P$  and  $D$  shells are shown in Fig. 1. In the figures, marks and solid lines stand for the empirical data and the fitted values, respectively. The cross section of  $pp$  scattering is fitted by the nucleon-nucleon potential  $U_{NN}$  as

$$U_{NN}(r) = V_{NN}(r) + i\alpha V_{NN}(r) \quad (8)$$

$$V_{NN}(r) = V_0 \exp(-r^2/a_0^2) + V_1 \exp(-r^2/a_1^2) \quad (9)$$

where,  $V_0$ ,  $V_1$ ,  $a_0$ ,  $a_1$  and  $\alpha$  are parameters obtained by fitting. The nucleon-nucleon cross section by the fitted phase shift value is represented in Fig. 2. Figures 3 and 4 show the parameters of Eqs. (6) and (7) as a function of the incident energies. Then, the Dirac optical potential is represented by

$$U_{opt}(r) = \int \frac{d^3\vec{q}}{(2\pi)^3} e^{i\vec{q}\cdot\vec{r}} \hat{u}_{opt}(q) \quad (10)$$

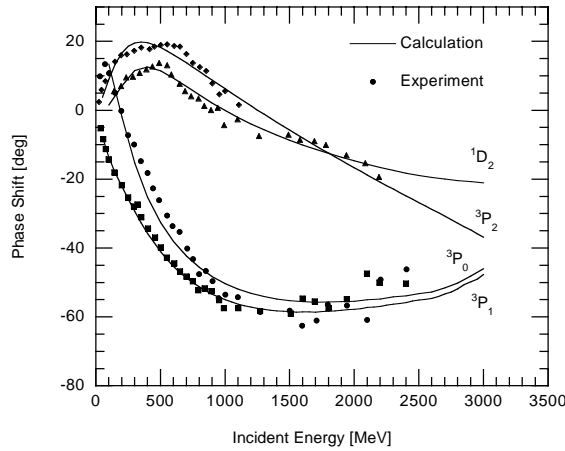


Fig. 1: Phase shift of  $P$  and  $D$  shell for  $p-p$  and  $p-n$  scattering. Solid marks stand for the values derived from the experimental data. Solid lines show the values by fitting.

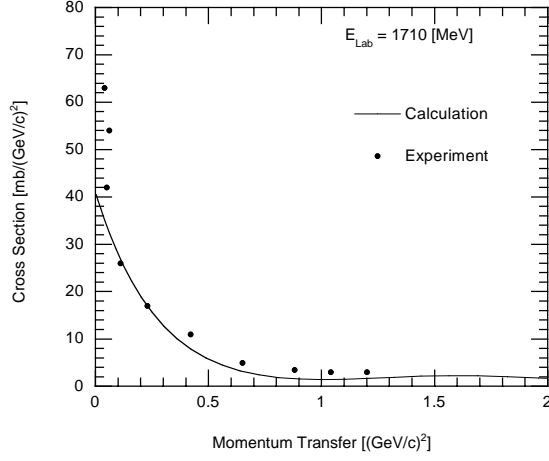


Fig. 2:  $p - p$  scattering cross section for collision energy of 1710 MeV. Solid marks stand for the values derived from the experimental data. Solid lines show the values by fitting.

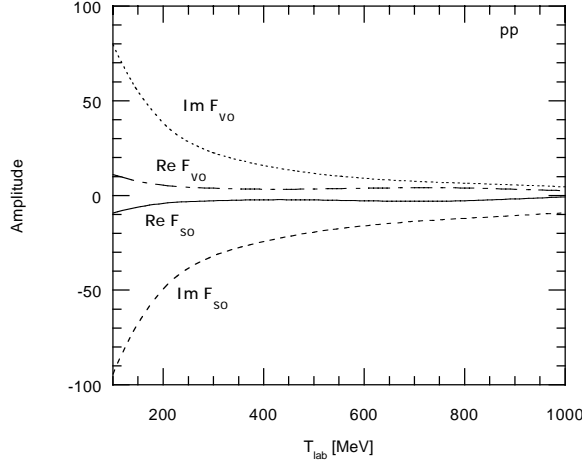


Fig. 3: Parameters of  $F_{S0}$  and  $F_{V0}$  of equations (6) and (7).

In figs. 5 and 6, the Dirac optical potential of the lead target for 500 MeV neutron incidence and the copper one for 1000 MeV incidence are represented, respectively.

To simplify the calculation, Dirac equation is converted to Shrödinger form as follows,

$$[p^2 + 2E(U_{cent} + U_{so}\vec{\sigma} \cdot \vec{L})]\Phi(r) = [(E - V_c)^2 - m]\Phi(r) \quad (11)$$

where  $p$  is momentum,  $m$  mass,  $E$  total energy,  $\vec{\sigma}$  spin,  $\vec{L}$  orbital momentum,  $V_c$  coulomb potential,  $U_S$  and  $U_V$  Dirac scalar and vector potential, respectively. The central and spin orbit potentials  $U_{cent}$ , and  $U_{so}$  are represented as,

$$U_{cent} = \frac{1}{2E}(2EU_V + 2mU_S - U_V^2 + U_S^2 - 2V_cU_V + 2EU_{Darwin}) \quad (12)$$

$$U_{so} = -\frac{1}{2EBr} \frac{\partial B}{\partial r} \quad (13)$$

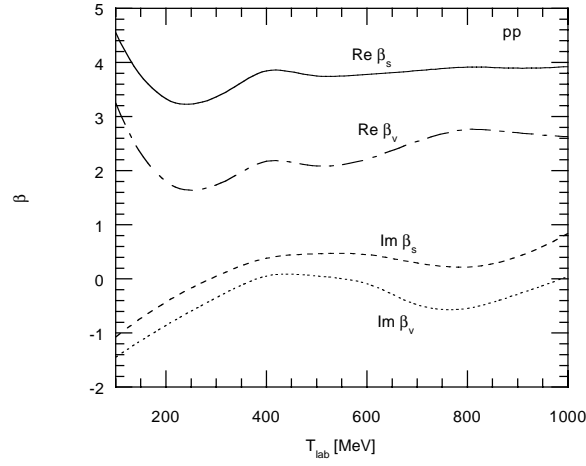


Fig. 4: Parameters of  $\beta_S$  and  $\beta_V$  of equations (6) and (7).

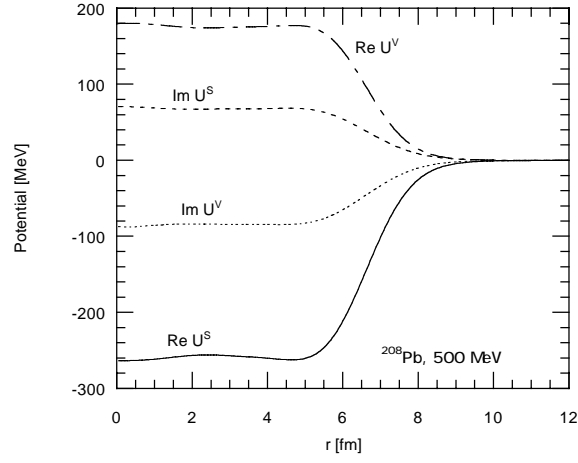


Fig. 5: The scalar and vector potentials for 500 MeV neutron incidence on  $^{208}\text{Pb}$  target.

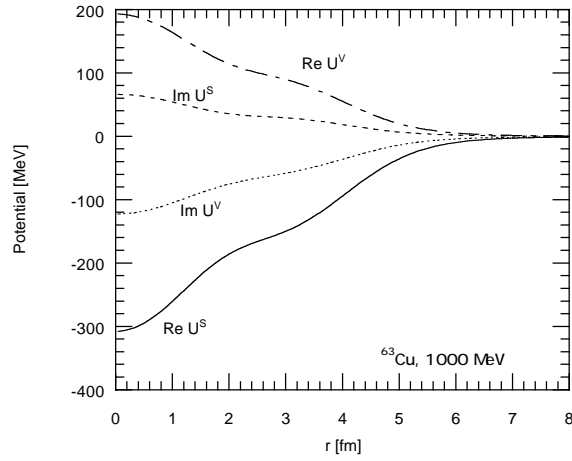


Fig. 6: The scalar and vector potentials for 1000 MeV neutron incidence on  $^{63}\text{Cu}$  target.

Darwin and  $B$  terms are

$$U_{\text{Darwin}} = -\frac{1}{2} \frac{1}{B r^2} \left( \frac{\partial}{\partial r} r^2 - \frac{\partial}{\partial r} B \right) + \frac{3}{4} \frac{1}{B} \left( \frac{\partial}{\partial r} B \right) \quad (14)$$

$$B = \frac{E + m + U_S - U_V - V_c}{E + m} \quad (15)$$

### 3. Calculation Results

Figure 7 shows the neutron incident total cross sections for  $^{239}\text{U}$ ,  $^{209}\text{Bi}$ ,  $^{208}\text{Pb}$ ,  $^{191}\text{Ta}$ ,  $^{107}\text{Ag}$  targets. Marks, dashed lines and solid ones stand for the experimental data [8], the results by global potential by Maruyama *et al.* [8] and by RIA, respectively. The proton incident reaction cross sections for  $^{209}\text{Pb}$ ,  $^{63}\text{Cu}$ ,  $^{40}\text{Ca}$ ,  $^{27}\text{Al}$  and  $^{12}\text{C}$  are shown in Fig. 8. Marks and solid lines are the experimental data [9] and the results by RIA. Figure 9 stands for the scattering cross section of  $^{40}\text{Ca}$  for 1044 MeV proton incidence. Marks and solid lines show the experimental data [8] and the results by RIA. In the Figs. 7 - 9 the cross sections by RIA are reproduced the experimental data.

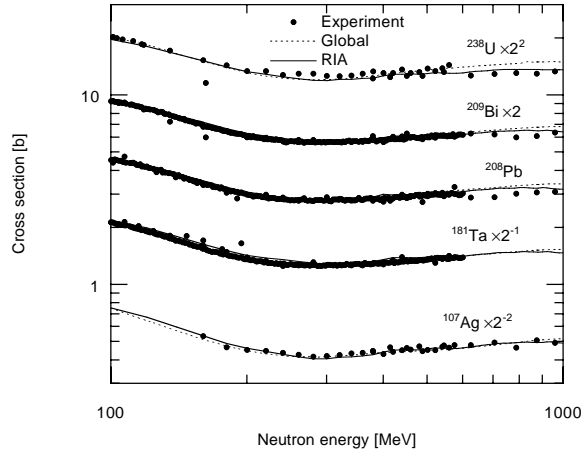


Fig. 7: Neutron incident total cross sections. Marks show the experimental data, dashed lines the global potential by Maruyama *et al.*, solid ones the results of RIA, respectively.

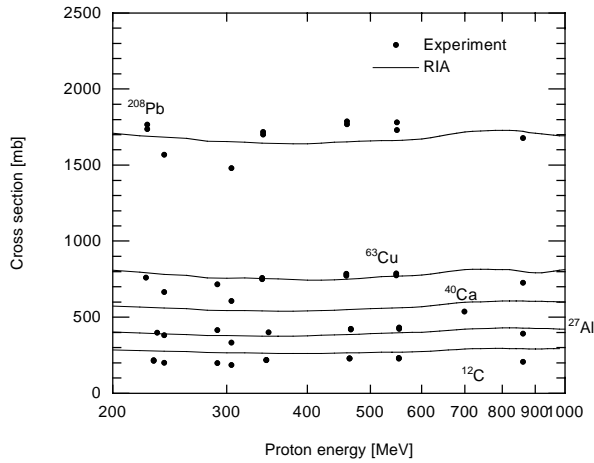


Fig. 8: Proton incident reaction cross sections. Marks show the experimental data, dashed lines the global potential by Maruyama *et al.*, solid ones the results of RIA, respectively.

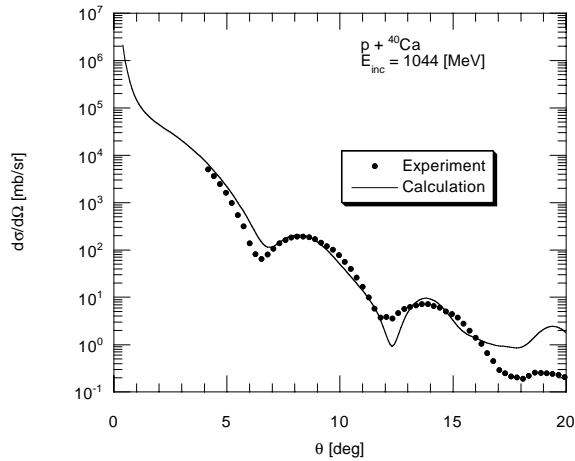


Fig. 9: Elastic scattering cross section of  $^{40}\text{Ca}$  for 1044 MeV proton incidence.

#### 4. Summary

Improvement of the neutron production cross section in the forward direction, the nucleon-nucleus Dirac optical potential obtained by RIA. The nucleon-nucleus Dirac optical potential is derived from the nucleon-nucleon scattering amplitude for each nucleon in the target nucleus. The nucleon-nucleon scattering amplitudes for each orbit are given by fitting empirical phase shift data. To simplify calculation of the potential, the neutron-proton and proton-proton scattering amplitudes are parameterized in a Gaussian shape as a function of the momentum transfer. The cross sections by this method are good agreement with the experimental data in high incident energy region.

#### References

- [1] Coleman W.A., *et al.*: *ORNL-4606* (1970).
- [2] Chandler K.C., and Armstrong T.W.: *ORNL-4744* (1972).
- [3] Bertini H.W., *et al.*: *Phys. Rev.*, **188**, 1711 (1969).
- [4] Horowitz C.J.: *Phys. Rev.*, **C31**, 1340 (1985).
- [5] McNeil J.A., *et al.*: *Phys. Rev.*, **C27**, 2123 (1983) and their in.
- [6] Arndt R.A., *et al.*: *Phys. Rev.*, **C28**, 97 (1983), *ibid*, **C56**, 3005 (1997).
- [7] Murdock D.P. and Horowitz C.J.: *Phys. Rev.*, **C31**, 538 (1985).
- [8] Maruyama S., *et al.*: *Proc. Int. Conf. Nuclear Data for Science and Technology*, 336, Trieste (1998), and their in.
- [9] Cooper E.D., *et al.*: *Phys. Rev.*, **C47**, 297 (1993) and their in.